Computer Modeling in Engineering & Sciences

Tech Science Press

DOI: 10.32604/cmes.2023.029878

ARTICLE

Mechanism of Thermally Radiative Prandtl Nanofluids and Double-Diffusive Convection in Tapered Channel on Peristaltic Flow with Viscous Dissipation and Induced Magnetic Field

Yasir Khan[1], Safia Akram[2,*], Maria Athar[3], Khalid Saeed[4], Alia Razia[2] and A. Alameer[1]

[1]Department of Mathematics, University of Hafr Al-Batin, Hafr Al-Batin, 31991, Saudi Arabia

[2]MCS, National University of Sciences and Technology, Islamabad, Pakistan

[3]SEECS, National University of Sciences and Technology, Islamabad, Pakistan

[4]College of Aeronautical Engineering, National University of Sciences and Technology, Islamabad, Pakistan

*Corresponding Author: Safia Akram. Email: drsafiaakram@gmail.com, drsafiaakram@mcs.edu.pk

Received: 12 March 2023 Accepted: 07 July 2023 Published: 17 November 2023

ABSTRACT

The application of mathematical modeling to biological fluids is of utmost importance, as it has diverse applications in medicine. The peristaltic mechanism plays a crucial role in understanding numerous biological flows. In this paper, we present a theoretical investigation of the double diffusion convection in the peristaltic transport of a Prandtl nanofluid through an asymmetric tapered channel under the combined action of thermal radiation and an induced magnetic field. The equations for the current flow scenario are developed, incorporating relevant assumptions, and considering the effect of viscous dissipation. The impact of thermal radiation and double diffusion on public health is of particular interest. For instance, infrared radiation techniques have been used to treat various skin-related diseases and can also be employed as a measure of thermotherapy for some bones to enhance blood circulation, with radiation increasing blood flow by approximately 80%. To solve the governing equations, we employ a numerical method with the aid of symbolic software such as Mathematica and MATLAB. The velocity, magnetic force function, pressure rise, temperature, solute (species) concentration, and nanoparticle volume fraction profiles are analytically derived and graphically displayed. The results outcomes are compared with the findings of limiting situations for verification.

KEYWORDS

Double diffusion convection; thermal radiation; induced magnetic field; peristaltic flow; tapered asymmetric channel; viscous dissipation; Prandtl nanofluid

Nomenclature

U, V	Velocities in X and Y directions
η_0	Viscosity of fluid
p_m	sum of magnetic and ordinary pressure
S_1	Strommer's number
R_m	Magnetic Reynolds numbers
(ξ, χ)	Prandtl fluid constraints

Rd	Thermal radiation
G_{rt}	Thermal Grashof number
p	Pressure
μ_e	Magnetic permeability
α	Channel half-width
(α_2 and α_3)	Amplitudes of left and right walls
S	Extra stress tensor for Prandtl fluid
ρ_f	Fluid density
$(\rho c)_f$	Heat capacity of fluid
β_T	Volumetric thermal expansion
ρ_p	Nanoparticle mass density
k	Thermal conductivity
Θ	Nanoparticle volume fraction
D_B	Brownian diffusion coefficient
D_s	Solutal diffusively
θ	Dimensionless temperature
D_{CT}	Soret diffusively
Re	Reynolds number
Ω	Nanoparticle volume fraction
γ	Dimensionless solutal concentration
ψ	Stream function
N_b	Brownian motion parameter
c	Propagation of velocity
N_{TC}	Dufour parameter
Le	Lewis number
Br	Brinkman number
Ec	Eckert number
E	Electricfield
N_{CT}	Soret parameter
k^*	Rosseland mean absorption
q_r	Radiative flux for radiation
λ	Wavelength
σ	Electric conductivity
t	Time
$(\widetilde{A}, \widetilde{B})$	Material constants of Prandtl fluid
ρ_{f_0}	Fluid density at T_0
$(\rho c)_p$	Heat capacity of nanoparticle
β_C	Volumetric solutal expansion
g	Acceleration due to gravity
T	Temperature
C	Solutal concentration
D_T	Thermophoretic diffusion coefficient
D_{TC}	Dufour diffusively
G_{rF}	Nanoparticle Grashof number
G_{rc}	Solutal Grashof number
σ^*	Stefan-Boltzmann constant
δ	Wave number

Pr	Prandtl number
Ln	Nanofluid Lewis number
N_t	Thermophoresis parameter

1 Introduction

The peristalsis flow of many physical fluids is significant natural phenomena that has vast industrial and medical applications. Peristalsis is the extension and condensation that naturally occurs on longitudinal walls of expandable chamber or tube. Human anatomy has numerous examples of the phenomenon among various organs such as stomach, large & small intestine, and others. The substances and liquids in human body move through peristalsis flow, hence the food digestion within gastrointestinal track, release of sperms and ovum by reproductory organs, blood circulation, lymph secretion and flow in lymphatic vessels, waste excretion through bladder and secretion of numerous hormones are all owe to the peristalsis. The same phenomenon is the life deriving force in plants too. Peristalsis extension and condensation appear in phloem relocation through sucrose suction within tubules. Other naturally occurring phenomena include propelling movements of insects. Moreover, in manufacturing industries, the phenomenon is implemented in devising medical equipment such as machines to pump blood, dialysis apparatus, finger pump machines, lung machinery and heart apparatuses. These applications attract the attention of many researchers to explore the peristaltic flow in human anatomy. In addition, its practical utility led many researchers and scientists like mathematicians, physicists, engineers to investigate the phenomenon actively and intensely. Some significant studies are referred in [1–10].

Another field of recent investigation is magneto-science which is the combination of biological systems and medical science with implications of a magnetic field. Many magnetic devices are available in the market like an instrument for cell segregation, bio-waste transportation equipment, gastrointestinal control through an induced magnetic field, drug targeting and trafficking devices, cancer cell control and destruction mechanism build through an alternating magnetic field are some of the examples of implication of the phenomenon in medical industry. Extension of this phenomenon is induced magnetic field (IMF) which is a supplementary magnetic flux induced upon electrically charged fluid with an external magnetic field. This occurrence owes to the effect of greater magnetic Reynolds number. IMF is applied in both medical and manufacturing industries, some of the examples include geophysics equipment, in MRI machines, glass production, electric MHD generators, etc. In medicine, the phenomenon has applications such as IMF combined with blood flows used in blood pumping, cardiac problems, and many other biological applications. Numerous studies have been conducted to theoretically and mathematically examine the phenomenon. Few recent works can be seen in [11–15].

Recently, researchers are engaged in exploring the techniques to ameliorate the thermos-physical qualities of fluids. One such technique is the addition of minute particles with increased heat conductivity [16]. If a liquid contains a large particle or nanoparticle, it cannot be stable and develop resistance to flow. If such kinds of fluids are injected into the human body, it will result in clotting and roughness. While nanoparticles ranging from 1–100 nm in a suspension can envelope more area with an increased coefficient of conduction and convection. Nanoparticles have vast engineering applications. Whereas in medicine, nanofluids are used in targeted drug transfer for cancer therapies and treatments. Kothandapani et al. [17] investigated the peristaltic nanofluids flow under magnetic flux and thermal radiation. While the numerous impacts of Jeffrey nanofluid with peristalsis have been examined by

Reddy et al. [18]. Ramesh et al. [19] further explored the phenomenon with couple stress fluid having magnetic flux and heat transfer. Recent literature on nanofluid flow has been listed as [20–27].

Thermal and concentration gradients involve in the process of double diffusion. The model was proposed by Aifanties [28] in 1976, according to which a concentration gradient is produced in a thermal mixture with sustained temperature difference. The phenomenon is useful in medical, engineering, and industrial solutions. Diffusion convection in peristaltic flow has numerous applications in the field of biomedicine. The cumulative impact of thermophoresis with Brownian motion under the magnetic force upon dual nonlinear thermal radiation was examined by Raju et al. [29]. Similarly, Ganesan et al. [30] explored the impact on non-Newtonian fluids. Further investigations on the flow of non-Newtonian fluid under double-diffusive convection are referred to in references [31–37].

The multiple advantages of thermal radiation impacts include the temperature control of a system, varying rate of heat transmission, thermal boundary layer control and regulating the structure of thermal layer. The investigation of Siddheshwar et al. [38] covers MHD flow with heat transfer of viscoelastic fluid over tense sheet in induced radiation. Aliakbar et al. [39] have examined the viscoelastic fluid flow through linear suspended sheet under the conditions of Maxwellian fluid and cross magnetic field. Similarly, Bataller [40] studied the flow of condensed second-grade liquid for non-isothermal stretched sheet with irregular heat production and absorption. Asha et al. [41] further explored the thermal radiation impact on Jeffrey's liquid peristaltic flow with double diffusion having gold nanoparticles. Whereas another study conducted by Farooq et al. [42] focused on hybrid nanomaterials of the peristaltic process of viscous liquid including slip effects, entropy increase and erratic radiation. Recent research on the topic is mentioned in references [43–49].

The impact of viscous dissolution on the rate of heat exchange is a notable energy source for continuous heat transfer. The quality and excellence of viscous dissolution are determined by whether the plate being used is heated or cooled. The material after heat processing mobile in wind rollers and feed rollers, and material produced through electronic chips, glass fibre, paper manufacturing, cooling of metals, etc., are examples of the process. Other related studies on viscous dissipation on peristalsis flow are given in [50–55].

In lieu of the above discussed implications of viscous dissipation, thermal radiation, nanofluid and double diffusion convection, the current investigation is to study the cumulative impact of viscous dissipation, thermal radiation, double diffusion convection on peristaltic flow of Prandtl nanofluid under induced magnetic flux in a tapered asymmetric channel. The present study in broader perspective deals with the blood circulation in vessels supposition of wall properties thermal radiation. The partial differential equation system has been resolved to couple ordinary differential equations through the lubrication method. The resultant equation is mathematically computed and then the resultant analysis is depicted graphically with altered parameters.

2 Mathematical Model

The following assumptions and approximations are used for the mathematical modelling of the present work:

- Two-dimensional and directional flow.
- Tapered asymmetric channel.
- Rosseland diffusion approximation for thermal radiation.
- Prandtl nanofluid.

- Induced magnetic field.

Let us assume the peristalsis of two-dimensional Prandtl nanofluid along the channel with width 2α. The flow originates like a sinusoidal wave propagation diffused with constant speed c along with asymmetric tapered channel. $H_1 = Y$ and $H_2 = Y$ are taken as the left and right walls of the tapered channel, respectively. The impact of thermal radiation, double diffusion convection, and viscous dissipation is assumed in the heat exchange. Then temperature, solute concentration, and nanoparticle volume fraction at the left and right walls are represented as T_0, C_0, Θ_0 and T_1, C_1, Θ_1, respectively. The velocity field, for two-dimensional & two-directional flow, is defined as $V = (U(X, Y, t), V(X, Y, t), 0)$. Moreover, an outer cross-uniform persistent magnetic field $\widetilde{H}_0$, induced magnetic field $\widetilde{H}_1^+ (h_X(X, Y, t), H_0 + h_Y(X, Y, t), 0)$ and cumulative magnetic field $\widetilde{H}^+ (h_X(X, Y, t), H_0 + h_Y(X, Y, t), 0)$ are considered. The schematic illustration of the problem is defined in Fig. 1.

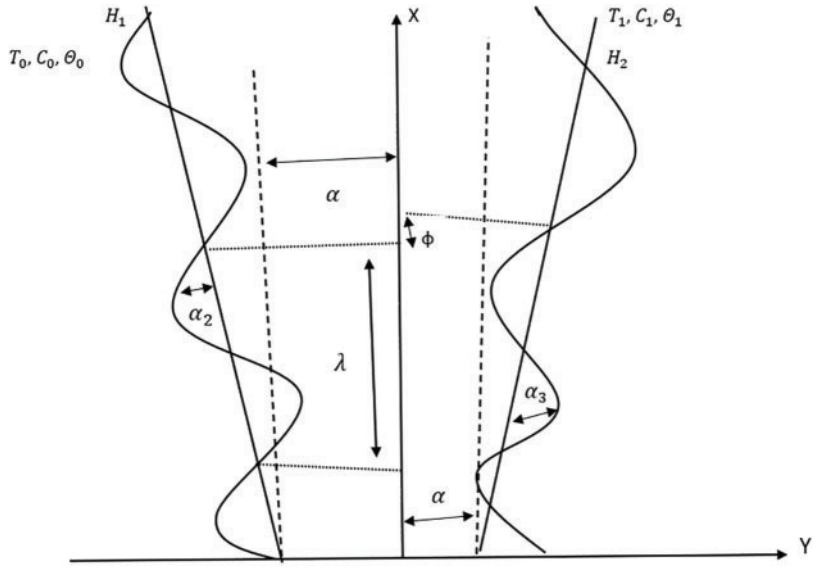

Figure 1: Schematic illustration of the problem

The tapered channel's left (H_1) and right (H_2) walls for a fixed reference frame are defined by [10,17]

$$Y = H_1 = -\alpha - \alpha_1 X - \alpha_2 \, sin\left[\frac{2\pi}{\lambda}(X - ct) + \varphi\right] = \text{(left wall)},$$
$$Y = H_2 = \alpha + \alpha_1 X + \alpha_3 \, sin\left[\frac{2\pi}{\lambda}(X - ct)\right] = \text{(right wall)}, \tag{1}$$

here α stands for channel half-width, $\alpha_1 (\alpha_1 << 1)$ indicates a non-uniform constant for tapered channel, α_2 and α_3 are amplitudes of the left and right walls respectively, t indicates time, c is the wave's phase speed, λ indicates wavelength, the phase difference φ lying between $[0, \pi]$. Also α_2, α_3, α, and φ satisfy the condition $\alpha_2^2 + \alpha_3^2 + 2\alpha_2\alpha_3 \, cos\, \varphi \leq (2\alpha)^2$.

For the Prandtl fluid, the Cauchy stress tensor is denoted by [37]

$$\tau = -p\boldsymbol{I} + \boldsymbol{S}, \tag{2}$$

$$\boldsymbol{S}=\left[\frac{\widetilde{A}\eta_0\ sin^{-1}\left[\frac{|\nabla \mathbf{V}|}{\widetilde{B}}\right]}{|\nabla \mathbf{V}|}\right]\nabla \mathbf{V}, \tag{3}$$

where $\boldsymbol{I}$ is identity tensor, p stands for pressure, $\boldsymbol{S}$ stands for extra stress tensor for Prandtl fluid, $(\widetilde{A},\ \widetilde{B})$ stands for material constants of Prandtl fluid.

The equations describing an incompressible, Prandtl nanofluid in laboratory frame $(X,\ Y)$ under the mechanism of double diffusivity convection, an induced magnetic field, radiation parameter and viscous dissipation are defined by [31]

$$\frac{\partial U}{\partial X}+\frac{\partial V}{\partial Y}=0, \tag{4}$$

$$\rho_f\left(\frac{\partial}{\partial \widetilde{t}}+U\frac{\partial}{\partial X}+V\frac{\partial}{\partial Y}\right)U=-\frac{\partial p}{\partial X}+\frac{\partial S_{XX}}{\partial X}+\frac{\partial S_{XY}}{\partial Y}+\mu_e\left(h_X\frac{\partial h_X}{\partial X}+h_Y\frac{\partial h_X}{\partial Y}+H_0\frac{\partial h_X}{\partial Y}\right)$$
$$-\frac{\mu_e}{2}\left(\frac{\partial H^{+2}}{\partial X}\right)+g\left\{(1-\Theta_0)\,\rho_{f0}\left\{\beta_T\,(T-T_0)+\beta_C\,(C-C_0)\right\}-\left(\rho_p-\rho_{f0}\right)(\Theta-\Theta_0)\right\}, \tag{5}$$

$$\rho_f\left(\frac{\partial}{\partial \widetilde{t}}+U\frac{\partial}{\partial X}+V\frac{\partial}{\partial Y}\right)V=-\frac{\partial p}{\partial Y}+\frac{\partial S_{YX}}{\partial X}+\frac{\partial S_{YY}}{\partial Y}-\frac{\mu_e}{2}\left(\frac{\partial H^{+2}}{\partial Y}\right)$$
$$+\mu_e\left(h_X\frac{\partial h_Y}{\partial X}+h_Y\frac{\partial h_Y}{\partial Y}+H_0\frac{\partial h_Y}{\partial Y}\right), \tag{6}$$

$$(\rho c)_f\left(\frac{\partial}{\partial \widetilde{t}}+U\frac{\partial}{\partial X}+V\frac{\partial}{\partial Y}\right)T=k\left(\frac{\partial^2 T}{\partial X^2}+\frac{\partial^2 T}{\partial Y^2}\right)+(\rho c)_p\left\{D_B\left(\frac{\partial \Theta}{\partial X}\frac{\partial T}{\partial X}+\frac{\partial \Theta}{\partial Y}\frac{\partial T}{\partial Y}\right)\right.$$
$$\left.\left(\frac{D_T}{T_0}\right)\left[\left(\frac{\partial T}{\partial X}\right)^2+\left(\frac{\partial T}{\partial Y}\right)^2\right]\right\}+D_{TC}\left(\frac{\partial^2 C}{\partial X^2}+\frac{\partial^2 C}{\partial Y^2}\right)-\frac{\partial q_r}{\partial Y}$$
$$+\left(S_{XX}\frac{\partial U}{\partial X}+S_{XY}\left(\frac{\partial U}{\partial Y}+\frac{\partial V}{\partial X}\right)+S_{YY}\frac{\partial V}{\partial Y}\right), \tag{7}$$

$$\left(\frac{\partial}{\partial \widetilde{t}}+U\frac{\partial}{\partial X}+V\frac{\partial}{\partial Y}\right)C=D_s\left(\frac{\partial^2 C}{\partial X^2}+\frac{\partial^2 C}{\partial Y^2}\right)+D_{CT}\left(\frac{\partial^2 T}{\partial X^2}+\frac{\partial^2 T}{\partial Y^2}\right), \tag{8}$$

$$\left(\frac{\partial}{\partial \widetilde{t}}+U\frac{\partial}{\partial X}+V\frac{\partial}{\partial Y}\right)\Theta=D_B\left(\frac{\partial^2 \Theta}{\partial X^2}+\frac{\partial^2 \Theta}{\partial Y^2}\right)+\left(\frac{D_T}{T_0}\right)\left(\frac{\partial^2 T}{\partial X^2}+\frac{\partial^2 T}{\partial Y^2}\right), \tag{9}$$

where ρ_{f_0}, g, β_C, ρ_f, β_T, $(\rho c)_p$, ρ_p, T, C, Θ, D_B, D_s, D_{CT}, $(\rho c)_f$, k, D_{TC}, D_T, symbolizes density of fluid at T_0, acceleration, volumetric solutal expansion coefficient, density of base fluid, volumetric thermal expansion of a fluid, heat capacity of nanoparticle, particles density, temperature, concentration, nanoparticle volume fraction, Brownian diffusion, solutal diffusively, Soret diffusively, fluid heat capacity, thermal conductivity, Dufour diffusively, and thermophoretic diffusion, respectively.

The radiative flux for radiation (q_r), stipulated in Eq. (7), is calculated by employing the Rosseland diffusion approximation and is given as [48]

$$q_r=-\frac{4\sigma^*}{3k^*}\frac{\partial T^4}{\partial Y}, \tag{10}$$

Since significant radiation limit is considered in this investigation. So, if temperature variations inside the flow path are negligibly small, T^4 is linear representation of temperature function and is modified by performing the Taylor expansion on T^4 about T_0 as shown below:

$$T^4 = T_0^4 + 4T_0^3 (T - T_0) + 6T_0^2 (T - T_0)^2 + \ldots, \tag{11}$$

By ignoring the higher powers of T (higher that first) in $(T - T_0)$, we get

$$T^4 = -3T_0^4 + 4T_0^3 T, \tag{12}$$

From Eqs. (10) and (12), we get

$$q_r = -\frac{16\sigma^* T_0^3}{3k^*} \frac{\partial T}{\partial Y}, \tag{13}$$

$$\frac{\partial q_r}{\partial Y} = -\frac{16\sigma^* T_0^3}{3k^*} \frac{\partial^2 T}{\partial Y^2}, \tag{14}$$

where σ^* represents Stefan-Boltzmann constant, and k^* represents Rosseland mean absorption.

$$x = \frac{X}{\lambda},\ m_0 = \frac{\alpha_2}{\alpha},\ u = \frac{U}{c},\ \delta = \frac{\alpha}{\lambda},\ m_1 = \frac{\alpha_3}{\alpha},\ p = \frac{\alpha^2 p}{\eta_0 c\lambda},\ t = \frac{c\bar{t}}{\lambda},\ M^2 = Re\ R_m S_1^2,\ h_1 = \frac{H_1}{\alpha},$$
$$y = \frac{Y}{\alpha},\ \mathrm{v} = \frac{V}{c}, m_2 = \frac{\alpha_1 \lambda}{\alpha},\ Re = \frac{\rho_f c\alpha}{\eta_0},\ \Theta = \frac{T - T_0}{T_1 - T_0},\ R_m = \sigma \mu_e \alpha c,\ Br = EcPr, \upsilon = \frac{\eta_0}{\rho_f},$$
$$\overline{\Phi} = \frac{\Phi}{H_0 \alpha},\ S_{xx} = \frac{\lambda S_{XX}}{\eta_0 c},\ S_{xy} = \frac{\alpha S_{XY}}{\eta_0 c},\ S_{yy} = \frac{\alpha S_{YY}}{\eta_0 c},\ \gamma = \frac{C - C_0}{C_1 - C_0},\ Pr = \frac{(\rho c)_f\ \upsilon}{k},\ Ln = \frac{\upsilon}{D_B},$$
$$p_m = p + \frac{1}{2} Re\ \delta \frac{\mu_e (H^+)^2}{\rho c^2}, \Omega = \frac{\Theta - \Theta_0}{\Theta_1 - \Theta_0}, Le = \frac{\upsilon}{D_s}, N_{CT} = \frac{D_{CT} (T_1 - T_0)}{(C_1 - C_0) D_s},\ u = \frac{\partial \psi}{\partial y},$$
$$S_1 = \frac{H_0}{c} \sqrt{\frac{\mu_e}{\rho}}, v = -\delta \frac{\partial \psi}{\partial x},\ h_y = -\delta \frac{\partial \Phi}{\partial x},\ N_{TC} = \frac{D_{CT} (C_1 - C_0)}{k (T_1 - T_0)}, N_b = \frac{(\rho c)_p D_B (\Theta_1 - \Theta_0)}{k},$$
$$N_t = \frac{(\rho c)_p D_T (T_1 - T_0)}{T_0 k},\ G_{rF} = \frac{g (\rho_p - \rho_f) (\Theta_1 - \Theta_0)}{\eta_0 c} \alpha^2, G_{rc} = \frac{(1 - \Theta_0) \rho_f \beta_c (C_1 - C_0) \alpha^2 g}{\eta_0 c},$$
$$G_{rt} = \frac{g\alpha^2 (1 - \Theta_0) \rho_f \beta_T (T_1 - T_0)}{\eta_0 c},\ Rd = -\frac{16\sigma^* T_0^3}{3k^*}. \tag{15}$$

Using Eq. (15), Eq. (4) is automatically satisfied, but Eqs. (5) to (9) along with Eq. (14) in wave frame becomes

$$Re\ \delta \left(\psi_{ty} + \psi_y \psi_{xy} - \psi_x \psi_{yy}\right) = -\frac{\partial p_m}{\partial x} + \delta^2 \frac{\partial S_{xx}}{\partial x} + \frac{\partial S_{xy}}{\partial y} - Re\ S_1^2 \Phi_{yy}$$
$$- Re\ S_1^2 \delta \left(\Phi_y \Phi_{xy} - \Phi_x \Phi_{yy}\right) + G_{rt} \Theta + G_{rc} \gamma - G_{rF} \Omega, \tag{16}$$

$$Re\ \delta^3 \left(\psi_{tx} + \psi_x \psi_{xy} - \psi_y \psi_{xx}\right) = -\frac{\partial p_m}{\partial y} + \delta^2 \frac{\partial S_{xy}}{\partial x} + \delta \frac{\partial S_{yy}}{\partial y} + Re\ \delta^2 S_1^2 \Phi_{yy}$$
$$- Re\ S_1^2 \delta^3 \left(\Phi_y \Phi_{xx} - \Phi_x \Phi_{xy}\right), \tag{17}$$

$$Re\ \delta\left(\Theta_t+\psi_y\Theta_x-\psi_x\Theta_y\right)=\frac{1}{Pr}\left(\Theta_{yy}+\delta^2\Theta_{xx}\right)+N_{TC}\left(\delta^2\gamma_{xx}+\gamma_{yy}\right)+Rd\Theta_{yy}$$
$$+Ec\left(\delta^2S_{xx}\psi_{xy}+S_{xy}\left(\psi_{yy}-\delta^2\psi_{xx}\right)-\delta S_{yy}\psi_{xy}\right)$$
$$+N_b\left(\delta^2\Omega_x\Theta_x+\Omega_y\Theta_y\right)+N_t\left(\delta^2\left(\Theta_x\right)^2+\left(\Theta_y\right)^2\right), \tag{18}$$

$$Re\ \delta Le\left(\gamma_t+\psi_y\gamma_x-\psi_x\gamma_y\right)=\left(\delta^2\gamma_{xx}+\gamma_{yy}\right)+N_{CT}\left(\delta^2\Theta_{xx}+\Theta_{yy}\right), \tag{19}$$

$$Re\ \delta Ln\left(\Omega_t+\Omega_x\psi_y-\Omega_y\psi_x\right)=\left(\delta^2\Omega_{xx}+\Omega_{yy}\right)+\frac{N_t}{N_b}\left(\delta^2\Theta_{xx}+\Theta_{yy}\right), \tag{20}$$

$$\psi_y-\delta\left(\psi_y\Phi_x-\psi_x\Phi_y\right)+\frac{1}{R_m}\left(\Phi_{yy}+\delta^2\Phi_{xx}\right)=E, \tag{21}$$

where R_m stands for magnetic Reynolds numbers, γ signifies solutal (species) concentration, Le stands for Lewis number, Ω signifies nanoparticle fraction, S_1 stands for Strommer's number, E represents electric field, G_{rt} signifies thermal Grashof numbers, Ln represents nanofluid Lewis number, Pr indicates Prandtl number, G_{rc} denotes solutal Grashof numbers, N_t indicates thermophoresis parameter, N_{TC} represents Dufour parameter, N_b indicates Brownian motion, G_{rF} stands for nanoparticle Grashof numbers, N_{CT} denotes Soret parameter, Re denotes Reynolds number, Θ stand for temperature, and p_m is total pressure in the fluid, which is the sum of magnetic and ordinary pressure.

Now considering the hypotheses of a long wavelength ($\delta << 1$) and a small but finite Reynolds number, the Eqs. (16) to (21) becomes

$$0=-\frac{\partial p}{\partial x}+\frac{\partial S_{xy}}{\partial y}+Re\ S_1^2\Phi_{yy}+G_{rt}\Theta+G_{rc}\gamma-G_{rF}\Omega, \tag{22}$$

$$-\frac{\partial p}{\partial y}=0, \tag{23}$$

$$\frac{\partial^2\Theta}{\partial y^2}+N_{TC}Pr\frac{\partial^2\gamma}{\partial y^2}+N_bPr\left(\frac{\partial\Theta}{\partial y}\frac{\partial\Omega}{\partial y}\right)+N_tPr\left(\frac{\partial\Theta}{\partial y}\right)^2+RdPr\frac{\partial^2\Theta}{\partial y^2}$$
$$+Br\left(\xi\left(\frac{\partial^2\psi}{\partial y^2}\right)^2+\frac{\chi}{6}\left(\frac{\partial^2\psi}{\partial y^2}\right)^4\right)=0, \tag{24}$$

$$\frac{\partial^2\gamma}{\partial y^2}+N_{CT}\frac{\partial^2\Theta}{\partial y^2}=0, \tag{25}$$

$$\frac{\partial^2\Omega}{\partial y^2}+\frac{N_t}{N_b}\frac{\partial^2\Theta}{\partial y^2}=0, \tag{26}$$

$$\Phi_{yy}=R_m\left(E-\frac{\partial\psi}{\partial y}\right), \tag{27}$$

Now omitted pressure from Eqs. (22) and (23), the equation for the stream function becomes

$$\frac{\partial^2S_{xy}}{\partial y^2}-Re\ S_1^2R_m\frac{\partial^2\psi}{\partial y^2}+G_{rt}\frac{\partial\Theta}{\partial y}+G_{rc}\frac{\partial\gamma}{\partial y}-G_{rF}\frac{\partial\Omega}{\partial y}=0, \tag{28}$$

where

$$S_{xy}=\xi\frac{\partial^2\psi}{\partial y^2}+\frac{\chi}{6}\left(\frac{\partial^2\psi}{\partial y^2}\right)^3, \tag{29}$$

where $\xi = \frac{\widetilde{A}}{\eta_0 \overline{B}}$ and $\chi = \frac{\xi c^2}{\overline{B}^2 \alpha}$ denotes Prandtl fluid constraints.

The non-dimensional form of the boundary conditions is

$$\psi = -\frac{F}{2} \text{ at } y = h_1(x) = -1 - m_2 x - m_0 \sin[2\pi(x-t)+\varphi],$$

$$\psi = \frac{F}{2} \text{ at } y = h_2(x) = 1 + m_2 x + m_1 \sin[2\pi(x-t)],$$

$$\frac{\partial \psi}{\partial y} = 0 \text{ at } y = h_1(x) = -1 - m_2 x - m_0 \sin[2\pi(x-t)+\varphi],$$

$$\frac{\partial \psi}{\partial y} = 0 \text{ at } y = h_2(x) = 1 + m_2 x + m_1 \sin[2\pi(x-t)], \tag{30}$$

$$\Theta = 0, \quad \Omega = 0, \quad \gamma = 0, \text{ at } y = h_1(x), \tag{31}$$

$$\Theta = 1, \quad \Omega = 1, \quad \gamma = 1, \text{ at } y = h_2(x), \tag{32}$$

$$\Phi = 0 \text{ at } y = h_1(x) \text{ and } y = h_2(x). \tag{33}$$

Volume flow rate:

When a period $T = \lambda/c$ is taken into consideration, the time-averaged flow at fixed point X is given by

$$Q_1 = \frac{1}{T}\int_0^T \overline{Q_1} dt. \tag{34}$$

we now acquire

$$Q_1 = q + \alpha_2 c \sin\left[\frac{2\pi}{\lambda}\left(X - c\bar{t}\right)\right] + \alpha_3 c \sin\left[\frac{2\pi}{\lambda}\left(X - c\bar{t}\right) + \varphi\right]. \tag{35}$$

where $q = \int_{H_1}^{H_2} u(x,y)\, dy$ is the wave frame's dimensional volume flow rate. Using non-dimensional mean flows Q in wave frame and F in laboratory frame, we have

$$F = \frac{Q_1}{c\alpha}, \; Q = \frac{q}{c\alpha}, \tag{36}$$

$$F(X,t) = Q + m_0 \sin[2\pi(x-t)] + m_1 \sin[2\pi(x-t)+\varphi], \tag{37}$$

where

$$F = \int_{h_1}^{h_2} u\, dy = \int_{h_1}^{h_2} \frac{\partial \psi}{\partial y} dy = \psi(h_2) - \psi(h_1). \tag{38}$$

The pressure rise per wave length Δp are described by

$$\Delta p = \int_0^1 \int_0^1 \left(\frac{\partial p}{\partial x}\right)_{y=0} dx dt. \tag{39}$$

3 Methodology of Solutions and Discussion

Numerical simulations are necessary because there are few cases for which analytic solutions can be found. Numerical simulations give us an alternative way to comprehend the issue and the solution without squandering the study's actual resources. We can have a thorough grasp of the flow circumstances by employing contemporary technologies, such as software like MATHEMATICA, MATLAB, and ANSYS. The coupled and non-linear properties of the Eqs. (22)–(28) make it difficult to evaluate the exact solutions. Thus, using MATHEMATICA's built-in command ND-Solve, the regressive equations are numerically solved. Solutions are used to calculate temperature, pressure gradients, concentration, pressure rises, nanoparticle volume fraction, magnetic force function, and streamlines for various flow parameters.

The biophysical and graphical significance of various flow parameters on Prandtl nanofluids flow in a tapered channel are examined in Figs. 2 to 11. The temperature effects on Brinkman number Br, Brownian motion N_b, and Prandtl number Pr are explored in Figs. 2a–2c. It is evident from Fig. 2a that the Brinkman number Br has an increasing influence on temperature. The fundamental cause of the temperature rise is that as Br values rise, shear flow resistance also rises. This causes more heat to be generated owing to viscous dissipation effects, which raises the fluid's temperature. The enhancing Brownian motion values also cause an increase in the temperature profile (see Fig. 2b). It is noticeable that forces exerted on nanometer-sized particles are stochastic forces that accelerate the particle's Brownian motion. As a result of the intense stochastic force, the base fluid's internal energy has increased, because of which the temperature profile has risen. From Fig. 2c, it is depicted that the temperature increases with an increase in Prandtl numbers Pr because of the potent effects of viscous dissipation. The graphs in Figs. 3a–3d explore how Concentration affects the Brinkman number Br, Brownian motion N_b, Dufour parameter (N_{CT}) , and Prandtl number Pr. It can be shown in Fig. 3a that the concentration of fluid particles significantly reduces as the impact of Brinkman number Br increases. Similar effects are observed in the cases of Brownian motion N_b, Dufour N_{TC} number and Prandtl number Pr. As seen in Fig. 3b, N_b has a declining impact on nanoparticle concentration, causing the concentration distribution to drop due to the huge transport of nanoparticles from a hot to a cold location. Fig. 3c shows that raising the Dufour number N_{CT} increases fluid heat transfer, which affects the fluid's viscosity by reducing the temperature difference between the wall and the fluid. The concentration of nanoparticles falls as a result. Fig. 3d shows that increasing the Prandtl number causes a decrease in the concentration of nanoparticles. Figs. 4a to 4d illustrate the graphic evolution of the nanoparticle fraction for varying values of Brownian motion N_b, Brinkman number Br, thermophoresis N_t and Prandtl number Pr. It is illustrated in Fig. 4a that the increasing impact of Brownian motion N_b causes nanoparticle fraction to rise. Physically, the Brownian motion index is enhanced because of the simultaneous random motion of the fluid and nanoparticles, which raises the fluctuations of the nanoparticle volume fraction. Opposite effects are noticed for the case of Br, N_t and Pr. It is noted from Figs. 4b to 4d that enhancing impact of Br, N_t and Pr causes the decrease in nanoparticle fraction.

Figs. 5a to 5d depict the effects of various Reynold number Re, nanoparticle Grashof numbers G_{rF}, magnetic Reynolds number R_m and thermal Grashof number G_{rt} on flow velocity. It is noted in Fig. 5a that the flow of velocity enhances in the region $y \in [-1.2, 0]$ due to the increasing impact of Reynolds number. Physically, viscous forces become less significant as the Reynolds number rises, which reduces the propagation of velocity defects in the flow field. The opposite effects are noted in the region $y \in [0, 1.3]$. In this region, flow velocity increases due to the increasing impact of Re. As demonstrated seen in Figs. 5b and 5c, enhancing the effect of nanoparticle Grashof numbers G_{rF} and Reynolds number R_m causes the fluid velocity to increase when $y \in [-1.2, 0]$ but decrease when

$y \in [0, 1.3]$. The opposite characteristic is observed for the case of thermal Grashof number G_{rt}. The flow velocity drops when $y \in [-1.2, 0]$ but increases when $y \in [0, 1.3]$ due to increasing impact of G_{rt} (see Fig. 5d).

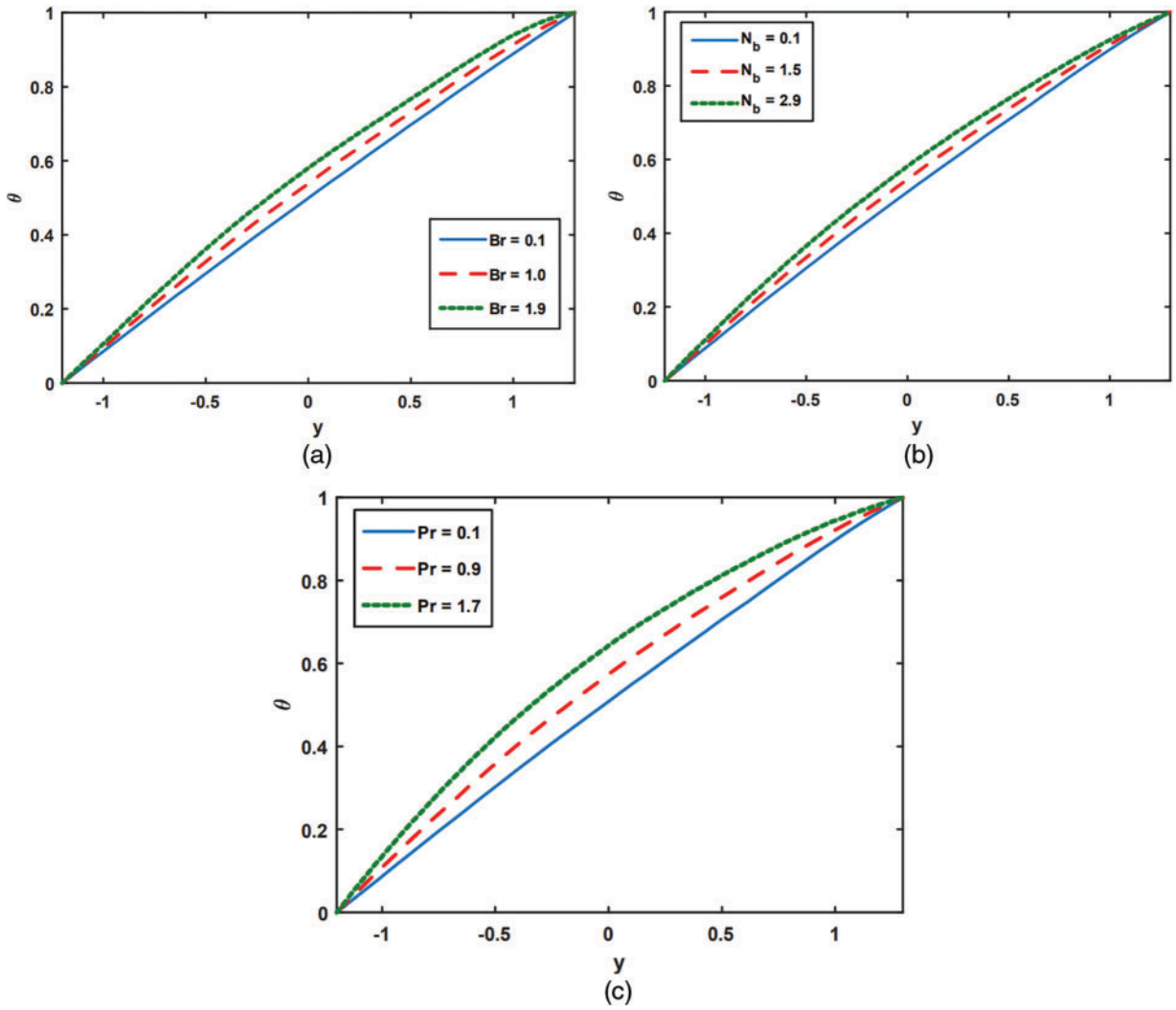

Figure 2: Temperature distribution for varying values of Br, N_b, and Pr

Figs. 6a to 6d are provided to illustrate how Br, Pr, G_{rF}, and Rd affect pressure gradients. The pressure gradient widens as the impact of Br and Pr increases (see Figs. 6a and 6b) but opposite impact is noted for the case of G_{rF}, and Rd. The pressure gradient drops as G_{rF}, and Rd increases (see Figs. 6c and 6d). Figs. 7a to 7c describe the outcomes of pressure rises on non-Newtonian parameters (χ and ξ), and nanoparticle Grashof number G_{rF}. To investigate the characteristic of pressure rise, pumping regions are split into the following categories: (a) when $Q > 0, \Delta p > 0$ the peristaltic zone occurs, where peristalsis oscillations govern pressure and fluid movement along their line of propagation; (b) when $Q > 0, \Delta p < 0$ the augmented zone occurs, where peristaltic push pressure boosts flow; (c) when $Q < 0, \Delta p > 0$ the retrograde zone exists, In this case, peristalsis is opposing the flow and (d) when $\Delta p = 0$ free pumping region exist. Here peristalsis walls are the only cause of flow in this

region. It is noted in Figs. 7a and 7b that the pressure rise increases in the retrograde region due to the increasing impact of non-Newtonian parameters (χ and ξ) but opposite effects are noted in peristaltic, augmented, and free pumping regions. Here pressure rise drops. It is noted in Fig. 7c that the pressure rise decreases in all the regions of peristaltic due to the increasing behaviour of G_{rF}. Figs. 8a and 8b are shown to highlight the analysis of R_m and E on the magnetic force function. It is to be observed in Figs. 8a and 8b that as R_m and E have a greater impact, the magnetic force function's magnitude values grow.

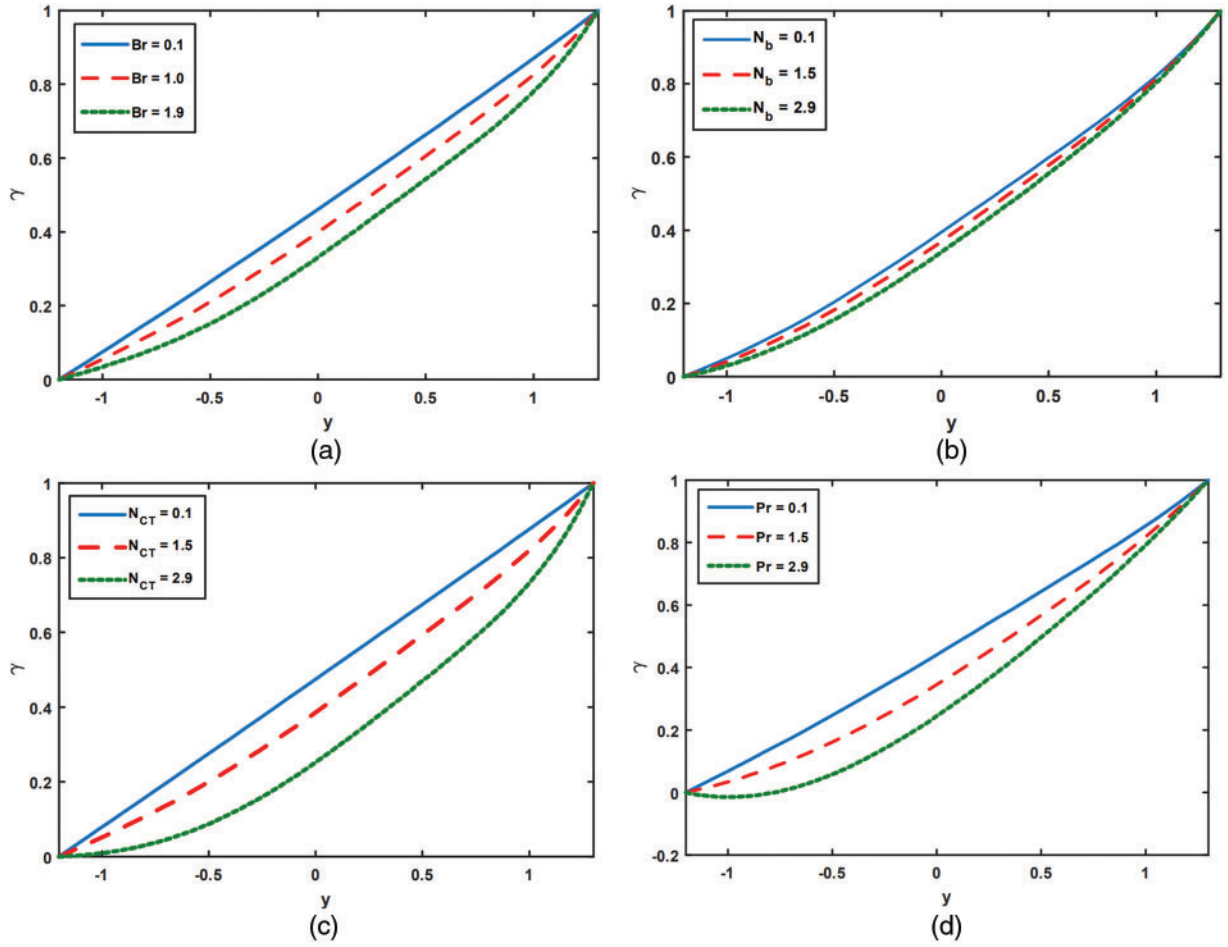

Figure 3: Concentration analysis for varying values of Br, N_b, N_{CT}, and Pr

To examine how trapping affects peristaltic flow, streamlines for G_{rF}, R_m, and G_{rt} are created. The streamlines are analyzed in Figs. 9 and 10 for varying values of nanoparticle Grashof G_{rF} and magnetic Reynolds number R_m. It is shown that as the influence of the nanoparticle Grashof G_{rF} and magnetic Reynolds number R_m grows, the size of the confined bolus decreases. By considering the thermal Grashof number, the opposite effects are observed (see Fig. 11). The thermal Grashof number (G_{rc}) here causes the confined bolus to grow in size.

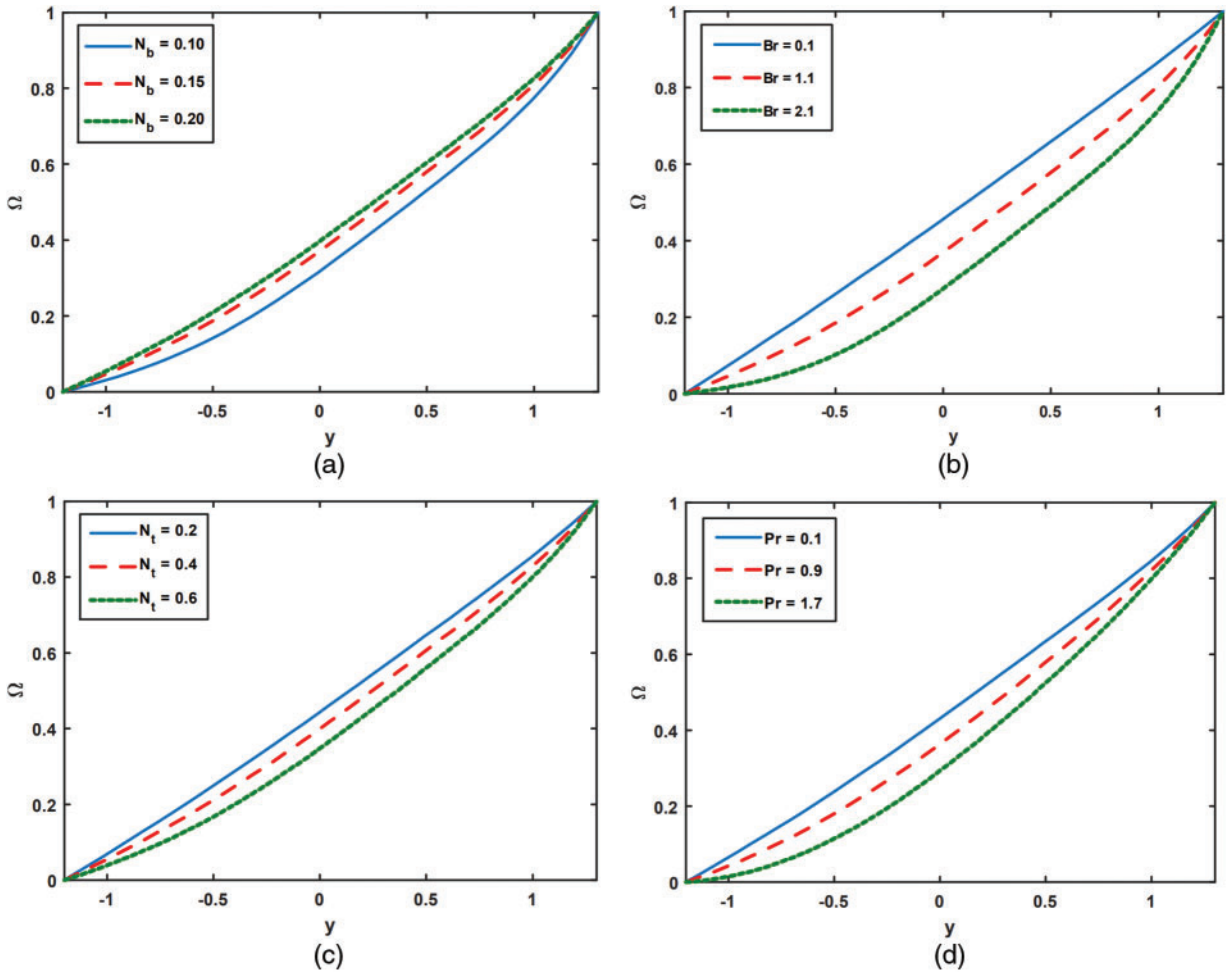

Figure 4: Analysis of N_b, Br, N_t and Pr on nanoparticle fraction

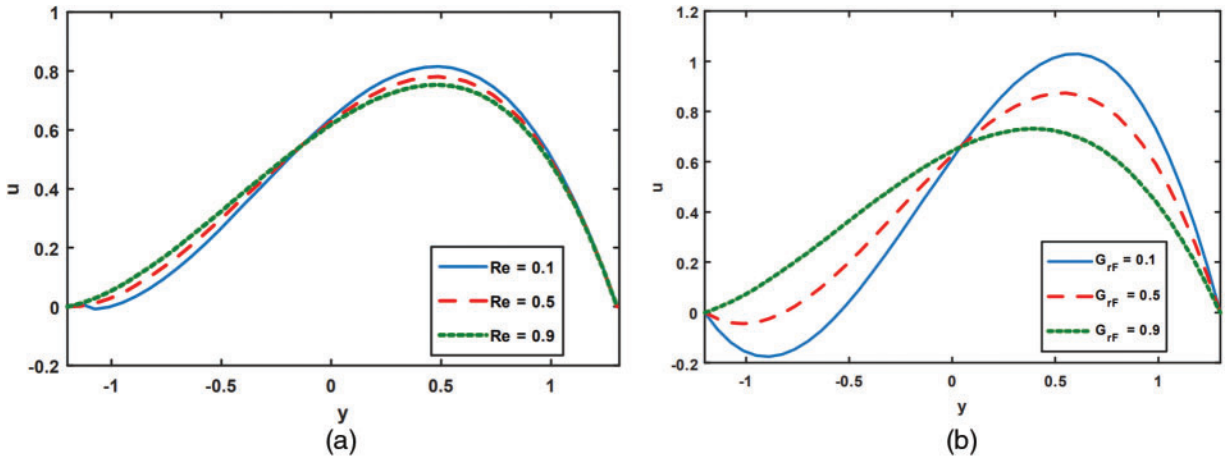

Figure 5: (Continued)

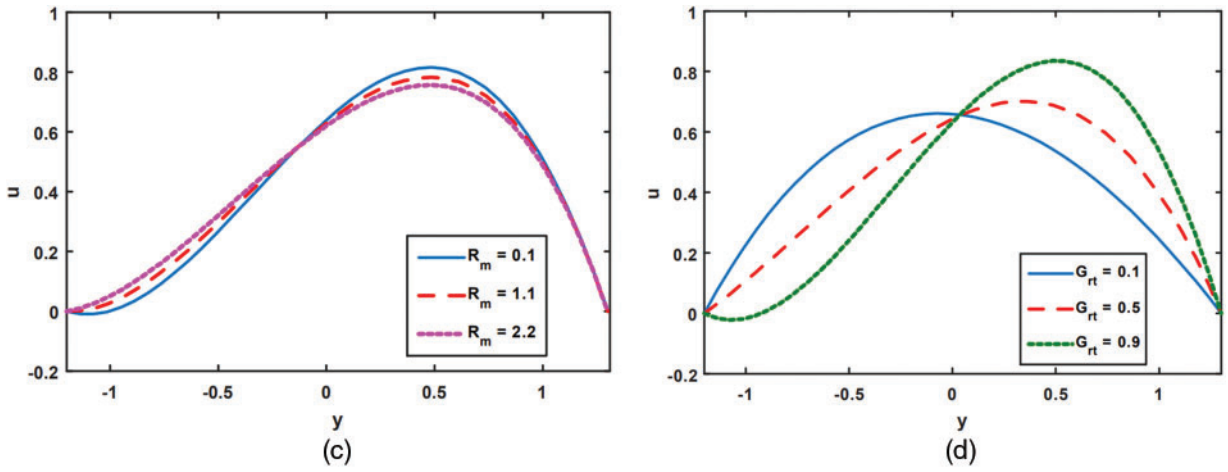

Figure 5: Effect of velocity for varying values of Re, G_{rF}, R_m and G_{rt}

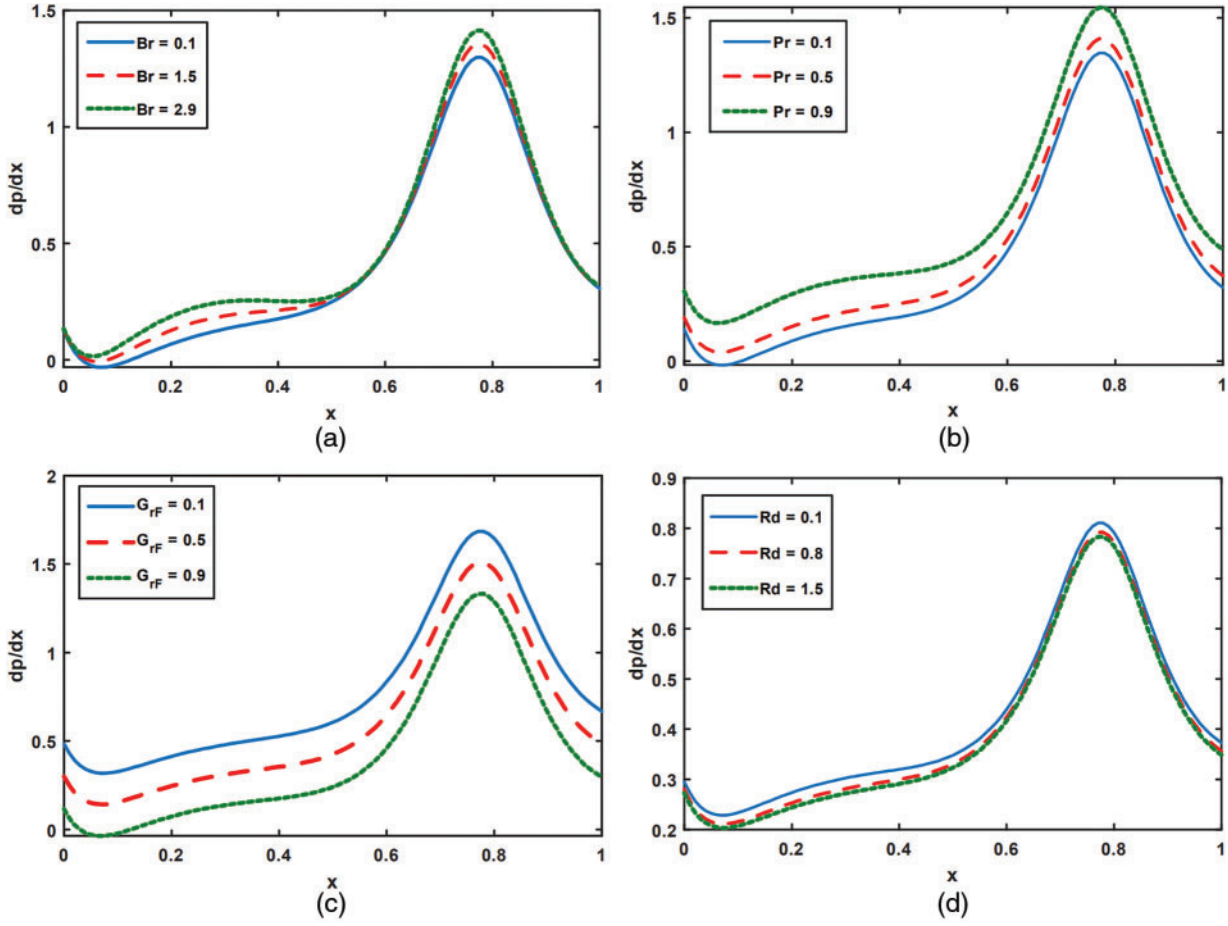

Figure 6: Analysis of Br, Pr, G_{rF}, and Rd on pressure gradient

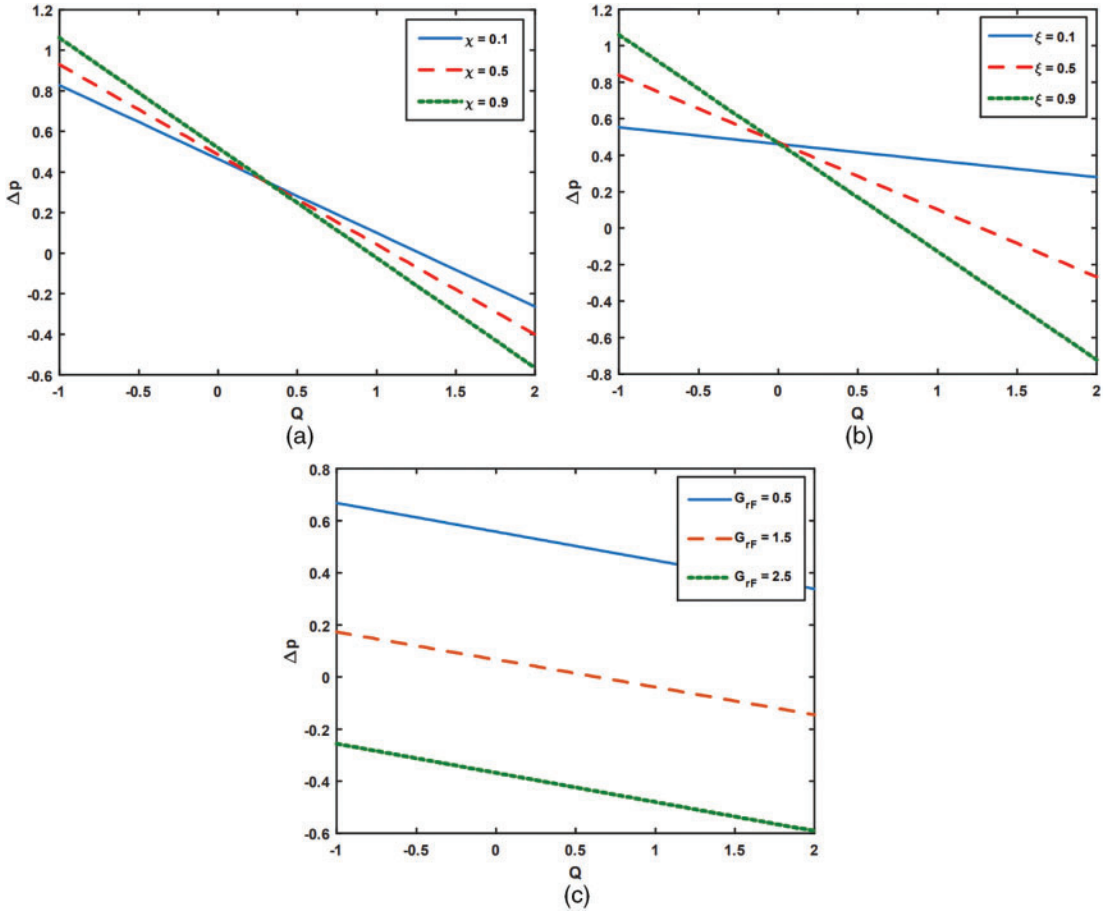

Figure 7: Impact of χ, ξ, and G_{rF} on pressure rise

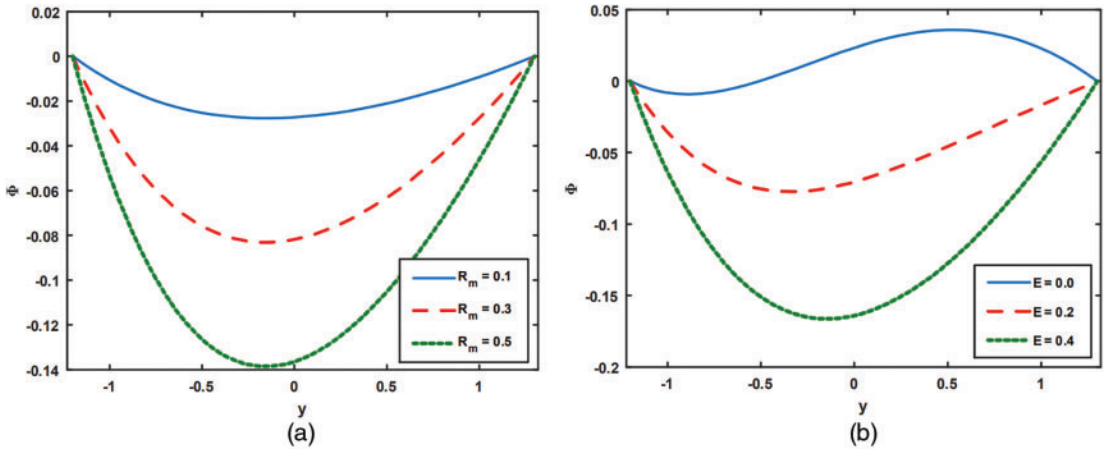

Figure 8: Analysis of R_m and E on magnetic force function

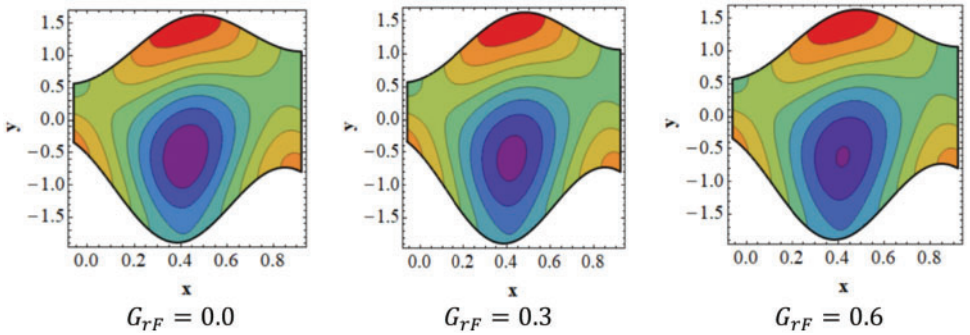

Figure 9: Analysis of G_{rF} on streamlines

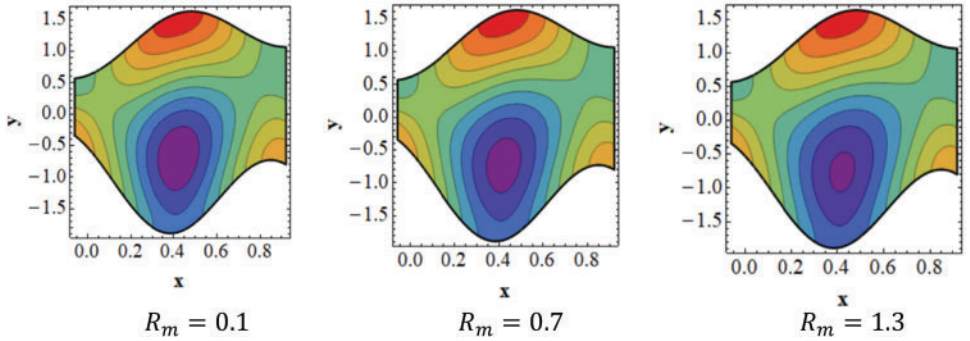

Figure 10: Analysis of R_m on streamlines

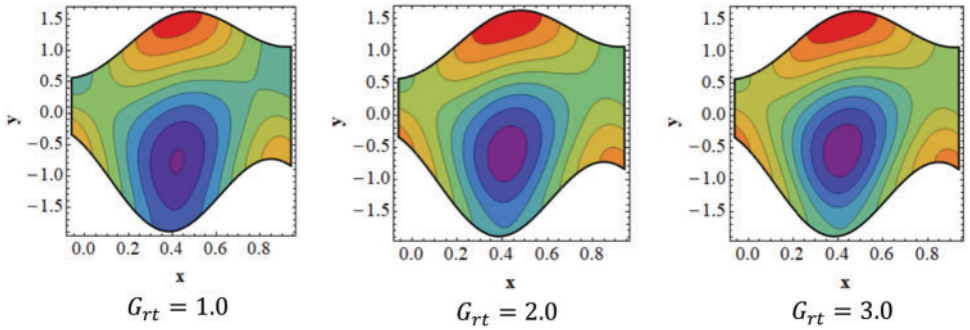

Figure 11: Analysis of G_{rt} on streamlines

4 Conclusion

In this article, we attempted to simultaneously link the consequences of thermal radiation and viscous dissipation with the influence of double diffusion convection on the peristaltic flow of magnetohydrodynamic Prandtl nanofluids in an asymmetric tapered channel. In our investigation, the equations governing the flow are developed using the preexisting constraints of long wavelength and low Reynolds values. Finally, reduced equations are solved numerically to achieve a comparative evaluation. It is observed that by raising Brinkman number the temperature of fluid flow increases because shear flow resistance increases. Furthermore, it is noted that increasing Brownian motion values accelerates the movement of nanoparticles along the fluid wall, which increases the temperature.

Another important finding is that due to the massive transit of nanoparticles from a hot to a cool, site Brownian motion has a diminishing effect on nanoparticle concentration, causing the concentration distribution to decrease. It is noted that by raising the effects of Reynolds number, viscous forces become less significant, which reduces the propagation of velocity defects in the flow field. Moreover, it is observed that by growing the influence of the nanoparticle Grashof and magnetic Reynolds number, the size of the confined bolus decreases.

Acknowledgement: Authors gratefully acknowledge technical and financial support from Ministry of Education and University of Hafr Al Batin, Saudi Arabia.

Funding Statement: This research work was funded by Institutional Fund Projects under No. (IFP-A-2022-2-5-24) by Ministry of Education and University of Hafr Al Batin, Saudi Arabia.

Author Contributions: The authors confirm contribution to the paper as follows: study conception and design: Y. K., S. A., A. A.; data collection: K. S., A. R., A. A.; analysis and interpretation of results: S. A., M. A., K. S.; draft manuscript preparation: S. A., A. R., Y. K.; funding: Y. K., A. A. All authors reviewed the results and approved the final version of the manuscript.

Availability of Data and Materials: No data was used for the research described in the article.

Conflicts of Interest: The authors declare that they have no conflicts of interest to report regarding the present study.

References

1. Latham, T. W. (1966). *Fluid motion in a peristaltic pump (M.S. Thesis)*. MIT, Cambridge, MA.
2. Tripathi, D., Bég, O. A., Gupta, P. K., Radhakrishnamacharya, G., Mazumdar, J. (2015). DTM simulation of peristaltic viscoelastic biofluid flow in asymmetric porous media: A digestive transport model. *Journal of Bionic Engineering, 12,* 643–655.
3. Sreenadh, S., Komala, K., Srinivas, A. N. S. (2017). Peristaltic pumping of a power–Law fluid in contact with a Jeffrey fluid in an inclined channel with permeable walls. *Ain Shams Engineering Journal, 8,* 605–611.
4. Mishra, M., Rao, A. R. (2003). Peristaltic transport of a Newtonian fluid in an asymmetric channel. *Zeitschrift fur Angewandte Mathematik und Physik (ZAMP), 54,* 532–550.
5. Nadeem, S., Akram, S. (2009). Peristaltic transport of a hyperbolic tangent fluid model in an asymmetric channel. *Zeitschrift für Naturforschung A, 64(9–10),* 559–567.
6. Ali, N., Abbasi, A., Ahmad, I. (2015). Channel flow of Ellis fluid due to peristalsis. *AIP Advances, 5,* 097214.
7. Mekheimer, K. S. (2002). Peristaltic transport of a couple stress fluid in a uniform and non-uniform channel. *Biorheology, 39,* 755–770.
8. Ellahi, R., Riaz, A., Nadeem, S., Ali, M. (2012). Peristaltic flow of Carreau fluid in a rectangular duct through a porous medium. *Mathematical Problems in Engineering, 2012,* 329639.
9. Vajravelu, K., Sreenadh, S., Devaki, P., Prasad, K. V. (2011). Mathematical model for a Herschel-Bulkley fluid flow in an elastic tube. *Central European Journal of Physics, 9,* 1357–1365.
10. Hayat, T., Akram, J., Zahir, H., Alsaedi, A. A. (2019). Peristaltic motion of Sisko fluid in an inclined asymmetric tapered channel with nonlinear radiation. *Journal of Thermal Analysis and Calorimetry, 138,* 545–558.
11. Vishnyakov, I., Pavlov, K. B., (1972). Peristaltic flow of a conductive liquid in a transverse magnetic field. *Magnetohydrodynamics, 8,* 174–178.

12. Munawar, S., Saleem, N. (2020). Second law analysis of ciliary pumping transport in an inclined channel coated with Carreau fluid under a magnetic field. *Coatings, 10,* 240.
13. Ellahi, R., Riaz, A., Sohail, S., Mushtaq, M. (2013). Series solutions of magnetohydrodynamic peristaltic flow of a Jeffrey fluid in eccentric cylinders. *Journal of Applied Mathematics & Information Sciences, 7,* 1441–1449.
14. Ellahi, R., Bhatti, M. M., Riaz, A., Sheikholeslami, M. (2014). Effects of magnetohydrodynamics on peristaltic flow of Jeffery fluid in a rectangular duct through a porous medium. *Journal of Porous Media, 17,* 143–157.
15. Akram, S., Nadeem, S. S., Hanif, M. (2013). Numerical and analytical treatment on peristaltic flow of Williamson fluid in the occurrence of induced magnetic field. *Journal of Magnetism and Magnetic Materials, 346,* 142–151.
16. Choi, S. U., Eastman, J. A. (1995). *Enhancing thermal conductivity of fluids with nanoparticles*. Argonne National Lab: Argonne, IL, USA.
17. Kothandapani, M., Prakash, J. (2015). Effects of thermal radiation parameter and magnetic field on the peristaltic motion of Williamson nanofluids in a tapered asymmetric channel. *International Journal of Heat and Mass Transfer, 81,* 234–245.
18. Reddy, M. G., Makinde, O. D. (2016). Magnetohydrodynamic peristaltic transport of Jeffrey nanofluid in an asymmetric channel. *Journal of Molecular Liquids, 223,* 1242–1248.
19. Ramesh, K., Devakar, M. (2015). Magnetohydrodynamic peristaltic transport of couple stress fluid through porous medium in an inclined asymmetric channel with heat transfer. *Journal of Magnetism and Magnetic Materials, 394,* 335–348.
20. Rahman, S. U., Ellahi, R., Nadeem, S., Zia, Q. M. Z. (2016). Simultaneous effects of nanoparticles and slip on Jeffrey fluid through tapered artery with mild stenosis. *Journal of Molecular Liquids, 218,* 484–493.
21. Akram, S., Nadeem, S. (2014). Significance of nanofluid and partial slip on the peristaltic transport of a Jeffrey fluid model in an asymmetric channel with different wave forms. *IEEE Transactions on Nanotechnology, 13,* 375–385.
22. Akram, S. (2014). Effects of nanofluid on peristaltic flow of a Carreau fluid model in an inclined magnetic field. *Heat Transfer Asian Research, 43,* 368–383.
23. Bhatti, M. M., Zeeshan, A., Ellahi, R. (2017). Simultaneous effects of coagulation and variable magnetic field on peristaltically induced motion of Jeffrey nanofluid containing gyrotactic microorganism. *Microvascular Research, 110,* 32–42.
24. Patil, P. M., Shankar, H. F. (2022). Heat transfer attributes of Al_2O_3–Fe_3O_4/H_2O hybrid nanofluid flow over a yawed cylinder. *Propulsion and Power Research, 11,* 416–429.
25. Ali, A., Barman, A., Das, S. (2022). EDL aspect in cilia-regulated bloodstream infused with hybridized nanoparticles via a microtube under a strong field of magnetic attraction. *Thermal Science and Engineering Progress, 36,* 101510.
26. Patil, P. M., Benawadi, S. (2022). Shape effects on the mixed convective hybrid nanoliquid flow over a rough slender cylinder with convective condition. *Waves in Random and Complex Media,* https://doi.org/10.1080/17455030.2022.2143930
27. Abbas, N., Shatanawi, W., Shatnawi, T. A. M. (2023). Thermodynamic study of radiative chemically reactive flow of induced MHD sutterby nanofluid over a nonlinear stretching cylinder. *Alexandria Engineering Journal, 70,* 179–189.
28. Aifanties, E. C. (1976). Continuum basis for diffusion in regions with multiple diffusivities. *Journal of Applied Physics, 50,* 1334–1338.
29. Raju, A., Ojjela, O., Kambhatla, P. K. (2020). The combined effects of induced magnetic field, thermophoresis and Brownian motion on double stratified nonlinear convective-radiative Jeffrey nanofluid flow with heat source/sink. *Journal of Analysis, 28,* 503–532.

30. Ganesan, S., Vasanthakumari, R. (2020). Influence of magnetic field and thermal radiation on peristaltic motion with double-diffusive convection in Jeffery nanofluids. *Heat Transfer, 49,* 2025–2043.
31. Bég, O. A., Tripathi, D. (2011). Mathematica simulation of peristaltic pumping with double-diffusive convection in nanofluids: A bio-nanoengineering model, proceedings of the institution of mechanical engineers. *Proceedings of the Institution of Mechanical Engineers, Part N: Journal of Nanomaterials, Nanoengineering and Nanosystems, 225,* 99–114.
32. Alolaiyan, H., Riaz, A., Razaq, A., Saleem, N., Zeeshan, A. et al. (2020). Effects of double diffusion convection on third grade nanofluid through a curved compliant peristaltic channel. *Coatings, 10(2),* 154.
33. Asha, S. K., Sunitha, G. (2020). Thermal radiation and hall effects on peristaltic blood flow with double diffusion in the presence of nanoparticles. *Case Studies in Thermal Engineering, 17,* 100560.
34. Sharma, A., Tripathi, D., Sharma, R. K., Tiwari, A. K. (2019). Analysis of double diffusive convection in electroosmosis regulated peristaltic transport of nanofluids. *Physica A: Statistical Mechanics and its Applications, 535,* 122148.
35. Akram, S., Afzal, Q. (2020). Effects of thermal and concentration convection and induced magnetic field on peristaltic flow of Williamson nanofluid in inclined uniform channel. *European Physical Journal Plus, 135,* 857.
36. Akram, S., Athar, M., Saeed, K., Razia, A., Muhammad, T. (2023). Hybridized consequence of thermal and concentration convection on peristaltic transport of magneto Powell–Eyring nanofluids in inclined asymmetric channel. *Mathematical Methods in the Applied Sciences, 46,* 11462–11478.
37. Akram, S., Athar, M., Saeed, K. (2021). Hybrid impact of thermal and concentration convection on peristaltic pumping of Prandtl nanofluids in non-uniform inclined channel and magnetic field. *Case Studies in Thermal Engineering, 25,* 100965.
38. Siddheshwar, P. G., Mahabaleshwar, U. S. (2005). Effects of radiation and heat source on MHD flow of a viscoelastic liquid and heat transfer over a stretching sheet. *International Journal of Non-Linear Mechanics, 40,* 807–820.
39. Aliakbar, V., Pahlavan, A. A., Sadeghy, K. (2009). The influence of thermal radiation on MHD flow of Maxwellian fluids above stretching sheets. *Communications in Nonlinear Science and Numerical Simulation, 14,* 779–794.
40. Bataller, R. C. (2007). Viscoelastic fluid flow and heat transfer over a stretching sheet under the effects of a non-uniform heat source, viscous dissipation and thermal radiation. *International Journal of Heat and Mass Transfer, 50(15–16),* 3152–3162.
41. Asha, S. K., Sunitha, G. (2019). Influence of thermal radiation on peristaltic blood flow of a Jeffrey fluid with double diffusion in the presence of gold nanoparticles. *Informatics in Medicine Unlocked, 17,* 100272.
42. Farooq, S., Khan, M. I., Waqas, M., Hayat, T., Alsaedi, A. (2020). Transport of hybrid type nanomaterials in peristaltic activity of viscous fluid considering nonlinear radiation, entropy optimization and slip effects. *Computer Methods Programs Biomed, 184,* 105086.
43. Mahmoud, M. A. A. (2007). Thermal radiation effects on MHD flow of a micropolar fluid over a stretching surface with variable thermal conductivity. *Physica A: Statistical Mechanics and its Applications, 375,* 401–410.
44. Mahantesh, M. N., Vajravelu, K., Abel, M. S. (2011). Heat transfer in MHD viscoelastic boundary layer flow over a stretching sheet with thermal radiation and non-uniform heat source/sink. *Communications in Nonlinear Science and Numerical Simulation, 16,* 3578–3590.
45. Jamshed, W., Devi, S. S. U., Goodarzi, M., Prakash, M., Nisar, K. S. et al. (2021). Evaluating the unsteady Casson nanofluid over a stretching sheet with solar thermal radiation: An optimal case study. *Case Studies in Thermal Engineering, 26,* 101160.
46. Jamshed, W., Nisar, K. S., Gowda, R. J. P., Kumar, R. N., Prasannakumara, B. C. (2021). Radiative heat transfer of second grade nanofluid flow past a porous flat surface: A single-phase mathematical model. *Physica Scripta, 96,* 064006.

47. Reddy, M. G., Padma, P., Shankar, B., Gireesha, B. J. (2016). Thermal radiation effects on MHD stagnation point flow of nanofluid over a stretching sheet in a porous medium. *Journal of Nanofluids, 5,* 753–764.
48. Nisar, Z., Hayat, T., Muhammad, K., Ahmed, B., Aziz, A. (2023). Significance of Joule heating for radiative peristaltic flow of couple stress magnetic nanofluid. *Journal of Magnetism and Magnetic Materials, 581,* 170951.
49. Hayat, T., Ahmed, B., Abbasi, F. M., Alsaedi, A. (2019). Numerical investigation for peristaltic flow of Carreau–Yasuda magneto-nanofluid with modified Darcy and radiation. *Journal of Thermal Analysis and Calorimetry, 137,* 1359–1367.
50. Abou-zeid, M. (2016). Effects of thermal-diffusion and viscous dissipation on peristaltic flow of micropolar non-Newtonian nanofluid: Application of homotopy perturbation method. *Results in Physics, 6,* 481–495.
51. Haile, E., Shankar, B. (2014). Heat and mass transfer through a porous media of MHD flow of nanofluids with thermal radiation, viscous dissipation and chemical reaction effects. *American Chemical Science Journal, 4,* 828–846.
52. Li, P., Abbasi, A., El-Zahar, E. R., Farooq, W., Hussain, Z. et al. (2022). Hall effects and viscous dissipation applications in peristaltic transport of Jeffrey nanofluid due to wave frame. *Colloid and Interface Science Communications, 47,* 100593.
53. Yassen, M. F., Mahrous, Y. M., Nazeer, M., Pasha, A. A., Hussain, F. et al. (2021). Theoretical study of transport of MHD peristaltic flow of fluid under the impact of viscous dissipation. *Waves in Random and Complex Media*. https://doi.org/10.1080/17455030.2022.2078519
54. Channakote, M. M., Kalse, V. D. (2022). Combined convective and viscous dissipation effects on peristaltic flow of Ellis fluid in non uniform tube. *Journal of Naval Architecture and Marine Engineering, 19,* 1–12.
55. Sadaf, H., Nadeem, S. (2017). Analysis of combined convective and viscous dissipation effects for peristaltic flow of Rabinowitsch fluid model. *Journal of Bionic Engineering, 14,* 182–190.